Null-Steering Antenna Design by Using Phase-Shifted Characteristic Modes

Francesco Alessio Dicandia, Simone Genovesi, *Member, IEEE*, and
Agostino Monorchio, *Fellow, IEEE*

***Abstract*—A novel low-cost null-steering antenna operating at 2.45 GHz is designed by exploiting an asymmetric excitation of two Characteristic Modes (CMs). This compact antenna allows a null shift of the radiation pattern by changing the relative phase between the two capacitive exciters (CCEs) located above the conductive plane. As a proof of concept, a prototype of the radiator has been realized by resorting to a discrete phase shifter in order to scan the null. The measured radiation patterns prove that the proposed design strategy is reliable and applicable to other kinds of structures. The manufactured antenna is capable to steer the null within a beam of 64° centered at broadside direction (θ = 0°), with depth nulls greater than 18 dB.**

***Index Terms*— Characteristic Mode (CM), reconfigurable antennas, null steering.**

I. INTRODUCTION

In a modern mobile communication system the use of reconfigurable antennas is a very important feature in order to improve the overall performance. The reconfigurability may involve the change of resonance frequency [1], [2], the radiation pattern [3], polarization [4] or a combination of them and it can be achieved by resorting to RF switches, photoconductive elements or mechanical alterations [5]. In general, frequency reconfigurable antennas allow frequency hopping and dynamic spectrum allocation, whereas both radiation pattern and polarization reconfigurability improve the communication system performance in coping with environment impairments. Among the pattern reconfigurable radiators, null-steering antennas represent an interesting subset in several applications. In fact, these antennas can cancel the effects of interferences coming from an intentional or a casual jammer by placing a pattern null in correspondence of the noise direction hence improving the signal-to-interference ratio (SIR) [6]. Some recent examples of such devices are represented by the antennas proposed in [7] and [8] where a microstrip patch employing twelve varactors realizes the null scanning in one principle plane and in 3D, respectively. The antennas have an overall dimension of 150 x 150 mm^2 and 154 x 154 mm^2 and a bandwidth between 2.37 GHz and 2.47 GHz. In [9] a slot antenna fed by a Wilkinson power divider exhibit a null-placing capability at 10 GHz. A two-port null-steering antenna operating in circular polarization (CP) is illustrated in [10] for mitigating intentional electromagnetic jamming in a GPS application. In this framework, one of the most challenging aspect consists of controlling the radiation pattern at a predetermined working frequency by exploiting a single antenna, thus avoiding any array configuration. Moreover, a pattern-reconfigurable antenna may necessitate a large size or require a matching network circuit.

A theoretical method useful to handle this design problem is represented by the Characteristic Mode Analysis (CMA) [11], [12]. In CMA the current distribution excited on a conductive body is represented as a linear superposition of several current modes. This comprehensive analysis allows visualizing and exploiting in the design process of an antenna not only the current distribution on the radiator itself but also the current flowing on the device in which the radiator is located. The contribution of this current can play a significant role in the overall antenna performance [13]. The usefulness of the CMA approach has been highlighted in several recent publications [14]–[18]. Generally, there are two options to excite a particular current mode on the structure: the former adopts inductive coupling elements (ICEs) whereas the latter employs capacitive coupling elements (CCEs). To properly excite a particular current mode distribution, an ICE has to be located at the maximum of the current mode distribution while the CCE has to be placed in correspondence of a minimum of the current mode distribution [19]. In [20], a three-port antenna system for small terminals is designed on the basis of a CMA and realized on a seven-layer PCB. In particular, eight ICEs are inserted in the device to excite three different current modes. On the contrary, the use of CCEs is illustrated in [21] to exploit the object hosting the antenna (*i.e.* a car chassis) for obtaining two working bandwidths, namely 0.7 GHz-0.96 GHz and 1.71 GHz-3.6 GHz. Moreover, both ICEs and CCEs are used in [22] to excite several modes of the structure and to minimize the isolation and the envelope correlation between them. The CM theory has been successfully applied also in many MIMO applications [23]–[26]. For example, two orthogonal radiation patterns are achieved in [27] by equally exciting two modes with 180° phase difference. In [28] the CMA of a smartphone chassis guided the design of a reconfigurable MIMO antenna that uses two tunable parasitic elements in order to modify the CM of the structure thus providing pattern diversity.

The aim of this paper is to propose a null-steering antenna exploiting current modes on a ground plane of the size of a mobile terminal. To achieve this goal, two current modes are asymmetrically excited by using two Capacitive Coupler Exciters (CCEs). The phase difference between the two exciting elements allows obtaining a null-steering radiator. The novel concept of the asymmetric excitation of current modes is realized by introducing a difference ($\Delta\theta$) in the phase associated to each CCE. The measured results prove that this antenna can steer the pattern null within a beam of 64°, centered at broadside direction (θ = 0°), with a null depth greater than 18 dB. As a

proof of concept, a prototype of the radiator that employs a discrete phase shifter has been realized in order to scan the null.

The paper is organized as follow. In Section II a brief overview of the CM theory, the antenna template and the asymmetric excitation concept are reported. The feeding network architecture is addressed in Section III whereas all the measurements on the fabricated prototype are reported in Section IV. Final conclusions are drawn in Section V.

II. Novel Characteristic Mode Excitation Paradigm

The novel excitation scheme adopted to achieve the null steering exploits some of the CMs of the structure to obtain different shapes of the radiation pattern. The first step consist of evaluating the CMs and the related radiation patterns. Next, it is necessary to choose among all the available patterns those that, once superimposed, guarantee the desired far field (*e.g.* a null in a certain direction). Next, the task is to find the number and suitable positions of the CCEs or ICEs that excite these modes. Finally, the selected modes can be asymmetric excited to produce the sweep of the beam.

A. Characteristic Modes Theory

The CMA represents the study of several current modes that a conducting body is able to support. The theory was first developed by Garbaz [11] and later redefined by Harrington [12]. Characteristic modes are obtained by solving an eigenvalue equation that is derived from the Method of Moments (MoM). The identified modes are independent of any kind of excitation and they only depend on the shape and the size of the investigated structure. These modes can be considered as a base to expand the total surface current (J_{tot}). In fact, J_{tot} can be written as a linear superposition of current modes:

$$J_{tot} = \sum_n \alpha_n J_n \tag{1}$$

where α_n denotes the Modal Weighting Coefficient (MWC) of the n^{th} characteristic mode and J_n represents its current distribution. Furthermore, α_n can be calculated as:

$$\alpha_n = \frac{V_n^i}{1 + j\lambda_n} \tag{2}$$

where λ_n is the eigenvalue associated to the n^{th} mode. The other two factors that contribute to the MWC are the Modal Significance (MS) of a mode, which is equal to:

$$MS = \left| \frac{1}{1 + j\lambda_n} \right| \tag{3}$$

and the Modal Excitation Coefficient (MEC) equal to:

$$V_n^i = \left\langle J_n, E^i \right\rangle = \oiint_S J_n \cdot E^i dS \tag{4}$$

where S is the surface of the conductive body and E^i the external excitation. Although the MS is independent of any kind of excitation, the term V_n^i takes into account the effect of the applied external excitation, including its position, magnitude and phase. Consequently, the inner product $\langle J_n, E^i \rangle$ quantifies the capacity of the applied source to excite the n^{th} current mode [12], [14].

B. Antenna Template

In the first design step, the CM analysis of the conducting plane, which mimics a handheld device of dimension 150 x 75 mm^2, has been performed in order to find the proper position of the CCEs to excite the useful current modes at 2.45 GHz. Since the purpose of this antenna is to provide a null steering, among all the current modes we are interested to excite only *Mode#4* and *Mode#8* (Fig. 1*a-b*). In fact, *Mode#4* presents a related pattern with a null in broadside direction ($\theta = 0°$), instead *Mode#8* presents a pattern null near $\theta = \pm 30°$ (Fig. 1*c-d*). The current orientation of these modes is along *y*-axis (red arrows) whereas black arrows represent the current amplitude. The polarization of the fields radiated by both current mode distributions is therefore linear along *y*-axis.

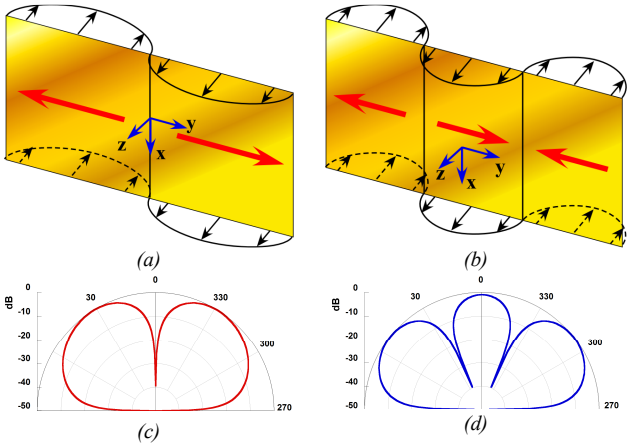

Fig. 1. Analysis of currents and patterns at 2.45 GHz for selecting the proper mode: current of *(a) Mode#4*, *(b) Mode#8* and radiation pattern related to *(c) Mode#4* and *(d) Mode#8*.

A sketch of the proposed antenna is illustrated in Fig. 2. It comprises a perfect conducting plane and two CCEs located in the middle of the shorter side where there is a current minimum. This allows the proper excitation of *Mode#4* and *Mode#8*. The rectangular exciters (5 x 32.5 mm^2) are placed parallel to the short side of the PEC plane at a height of 4 mm. A voltage source is set between the ground plane and each CCE center. The dimensions of two CCEs have been selected in order to provide a real input impedance.

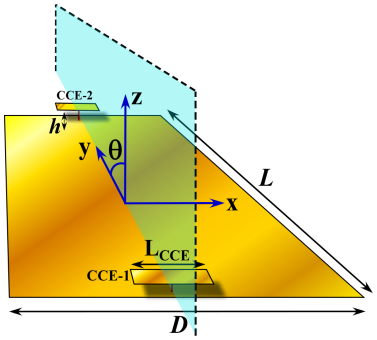

Fig. 2. View of the antenna template; *L = 150 mm, D = 75 mm, L_{CCE} = 32.5 mm, h = 4 mm*.

Afterwards, the overall structure has been analyzed in order to take into account also the exciters effect. The MS of the first eight modes of the whole antenna is shown in Fig. 3. MS allows understanding how much a particular mode (J_n) contributes to

the total current distribution (J_{tot}) and radiated power [30], if properly excited. It is evident that in the frequency range of interest most of the modes have a value near to one, except *Mode#5* and *Mode#6* which are higher order modes that store magnetic energy [12]. However, the position of the CCEs plays a fundamental role in excitation of *Mode#4* and *Mode#8*.

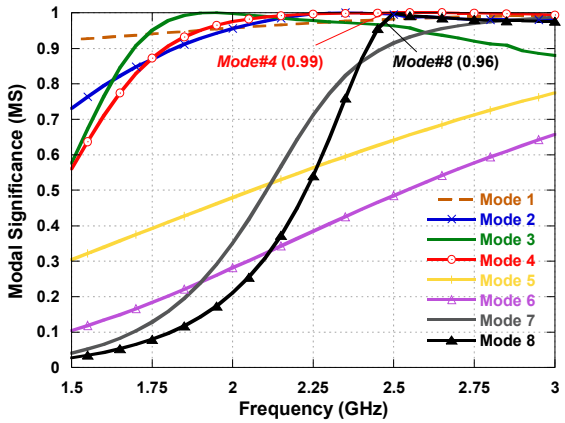

Fig. 3. Modal Significance of the antenna template with CCEs.

Let us first consider that each CCE is individually excited. As it is evident from the normalized MWC amplitude presented in Fig. 4*a*, it can be observed that *Mode#4* and *Mode#8* are both dominant when CCE-1 and CCE-2 are not simultaneously excited over the structure.

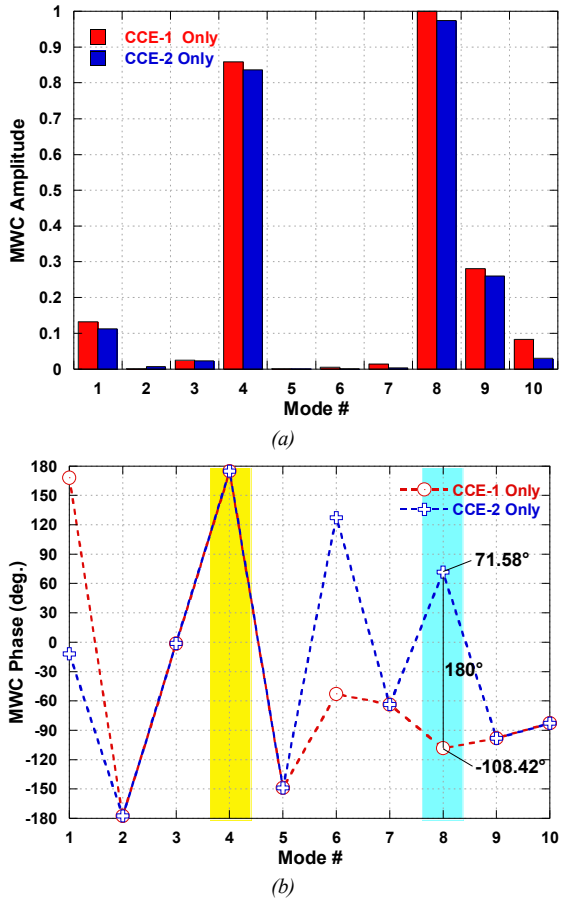

Fig. 4. *(a)* Normalize amplitude and *(b)* phase of the MWC when CCE-1 and CCE-2 are excited respectively at 2.45 GHz.

The reason why all the other modes present a MWC so small is due to the position and the kind of the exciters applied, as well as the eigenvalue (λ_n) associated to each mode. This happens because the other current modes do not present nearby the CCE a null of the current distribution. Therefore the coupling between the exciter and the n^{th} current mode, namely the MEC, results very low since the designed CCEs enable to excite properly only the modes that present a minimum of the current distribution nearby the exciters

An interesting consideration can be drawn looking at the phase of the MWC (Fig. 4*b*). It can be seen that the phase of the MWC associated to *Mode#4* when only CCE-1 is excited is the same as the phase of the MWC associated to *Mode#4* when only CCE-2 is excited (highlighted in yellow). If we look at the MWC phase related to *Mode#8* we find out that there is a 180° difference between the two aforementioned cases (only CCE-1 excited and only CCE-2 excited). The latter case is highlighted in cyan in Fig. 4*b*. This means that when both CCEs are excited in-phase ($\Delta\theta = 0°$), only *Mode #4* will be excited on the structure whilst if they are out-of-phase ($\Delta\theta = 180°$) only *Mode#8* will be stimulated.

Since each CCE is able to excite mainly *Mode#4* and *Mode#8*, if we call $J_{CCE\text{-}1}$ and $J_{CCE\text{-}2}$ the current distribution over the structure due to the CCE-1 and CCE-2 respectively, they can be approximated as:

$$\begin{cases} J_{CCE-1} = \sum_n \alpha_n J_n \cong \alpha_4 J_4 + \alpha_8 J_8 \\ J_{CCE-2} = \sum_n \beta_n J_n \cong \beta_4 J_4 + \beta_8 J_8 \end{cases} \quad (5)$$

where α and β represents the MWC associated to each mode due to the CCE-1 and CCE-2. Then, the total current distribution (J_{tot}) over the conducting plane can be obtained as a linear superposition of the current due to each exciters, namely:

$$J_{tot} \cong \left(\alpha_4 + \beta_4\right) J_4 + \left(\alpha_8 + \beta_8\right) J_8 \quad (6)$$

C. Asymmetric Excitation

From Fig. 4, we can approximate $|\alpha_4| \cong |\beta_4|, |\alpha_8| \cong |\beta_8|$ and assume $\arg(\alpha_4) = \arg(\beta_4), \arg(\alpha_8) = \arg(\beta_8) + \pi$. Then, by introducing a phase difference $\Delta\theta$ between the exciters, the total current distribution (J_{tot}) over the structure becomes:

$$J_{tot} = \left[2\alpha_4 e^{i\left(\frac{\Delta\theta}{2}\right)} \cos\left(\frac{\Delta\theta}{2}\right)\right] J_4 + \left[2\alpha_8 e^{i\left(\frac{\pi+\Delta\theta}{2}\right)} \sin\left(-\frac{\Delta\theta}{2}\right)\right] J_8 \quad (7)$$

From equation (7) it can be observed that when the exciters are in phase ($\Delta\theta = 0°$), the entire structure is able to excite *Mode#4* (current J_4), whereas by changing the delta phase $\Delta\theta$ the intensity of *Mode#4* decreases and *Mode#8* (current J_8) enhances more and more, up to become the main mode when the exciter are out of phase.

In order to prove that by changing the phase difference between the exciters the structure is able to modify the level of the excitation of *Mode#4* and *Mode#8*, the MWC (Fig. 5*a*) and the correlation ρ (Fig. 5*b*) between the entire radiation pattern and the first ten modes are reported with respect to the phase difference $\Delta\theta$. As reported in [13],[20], the correlation (ρ) is a

measure that describes how strongly a mode contributes to the total radiated field and it is evaluated by:

$$\rho_{total,n} = \frac{\alpha_n}{\sqrt{P_{rad}}} \tag{8}$$

where α_n represents the MWC and P_{rad} the total radiated power. From Fig. 5 it is apparent that by introducing the phase difference $\Delta\theta$ between the CCEs, the antenna is capable to modify the level of the coupling of *Mode#4* and *Mode#8*, whereas the other modes always remain very low. Moreover, this trend confirms that said before in the (7). Indeed, when the two CCEs are excited in phase ($\Delta\theta = 0°$) only *Mode #4* is excited over the structure. However, *Mode#4* fades little by little by increasing the phase difference whereas the *Mode#8* becomes gradually stronger, up to be the only mode excited over the structure when the phase difference is 180°. This fact is at the basis of the null-scanning property of the proposed antenna.

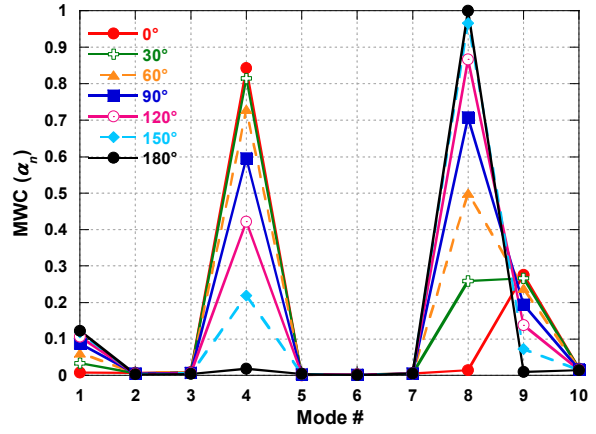

(a)

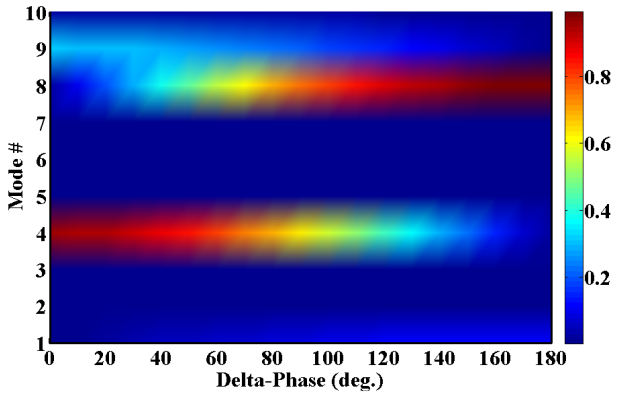

(b)

Fig. 5. *(a)* Modal Weighting Coeficient and *(b)* correlation ρ between the first ten modes and the entire radiation pattern as a function of phase difference $\Delta\theta$ at 2.45 GHz.

Finally, the surface current distribution on the rectangular plane is presented in Fig. 6 for $\Delta\theta \in (0°\text{-}180°)$ with step of 30°. As it is apparent, when the exciters are fed in-phase the current distribution resembles *Mode#4* whereas, when the CCEs are out of phase, it is very similar to *Mode#8*. In all the other cases within $\Delta\theta \in (0°, 180°)$ the current distribution is a weighted combination of both modes, as predicted by the CMA and the MWC observation (Fig. 5).

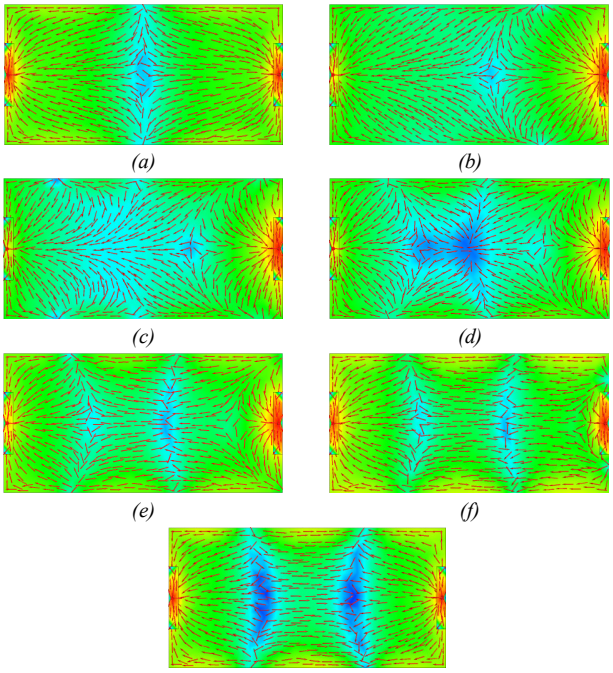

(a) *(b)* *(c)* *(d)* *(e)* *(f)* *(g)*

Fig. 6. Current distribution on the antenna by changing the relative phase; *(a)* $\Delta\theta = 0°$, *(b)* $\Delta\theta = 30°$, *(c)* $\Delta\theta = 60°$, *(d)* $\Delta\theta = 90°$, *(e)* $\Delta\theta = 120°$, *(f)* $\Delta\theta = 150°$, *(g)* $\Delta\theta = 180°$.

III. Feeding Network

A feeding network has been designed to provide the necessary differential-phase feeding for the two CCEs.

The variation of the input impedance of each CCE as a function of its length (L_{CCE}) has been preliminary taken into account as it is reported in Fig. 7. It can be observed that although the real part is almost constant for the most part of L_{CCE} values, the imaginary part is more sensible L_{CCE} increases quite regularly. A value of 32.5 mm has been selected for L_{CCE} to have an input impedance almost completely real in the frequency range 2.3 GHz-2.6 GHz for matching purpose. In this case the input impedance at 2.45 GHz is around 6 Ω, which can be easily matched to 50 Ω with the use a quarter-wave impedance transformer.

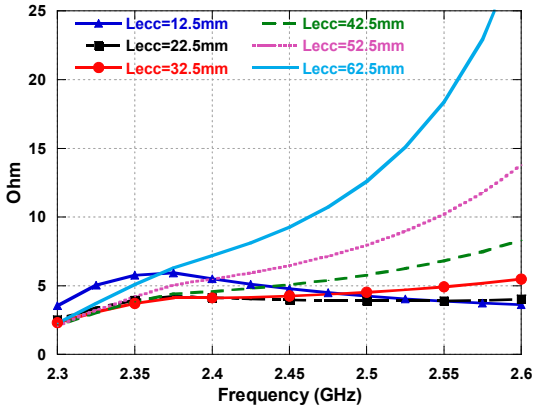

(a)

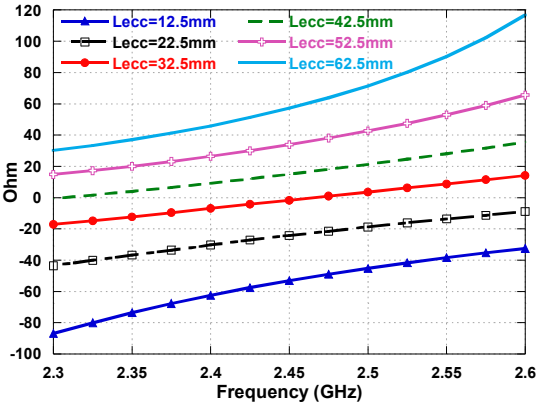

(b)

Fig. 7. Input impedance as a function of frequency of each CCE obtained by changing the total length L_{CCE}; *(a)* real part, *(b)* imaginary part.

Afterwards, a discrete phase shifter has been designed to provide a set of values for Δθ and it has been included in each branch of the feeding network. The layout is reported in Fig. 8 where the conductive rectangular plane is considered as the ground plane for the microstrip lines. The input port (Port #1) is connected to Port #2 and Port #3 through different-length paths that are selectable by using pin diodes. A quarter-wave transformer is used to efficiently connect the feeding network microstrip (50 Ω-line) to the capacitive exciters. The different paths allow changing the phase shift from 0° to 180° with a step of 30°.

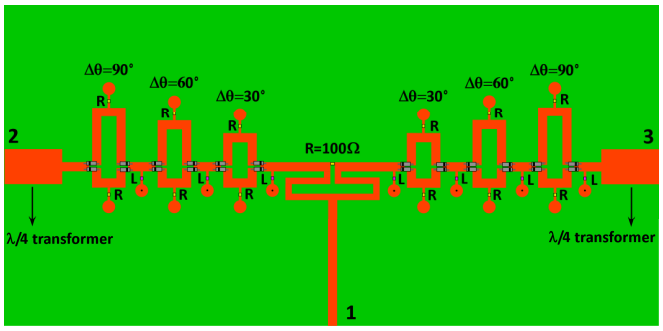

Fig. 8. Layout of the employed feeding network

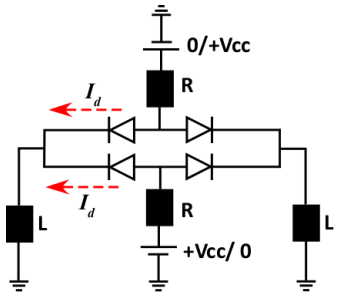

Fig. 9. DC biasing circuit for pin diodes

The feeding network has been printed on a 1.2mm-thick FR4 substrate and thin DC biasing lines were implemented to change the pin diodes (BAR50-02V) state of polarization, hence the relative phase (Δθ) between Port #2 and Port #3. In the simulations, each pin diode was modelled as a series R_d-L_d network (R_d = 3Ω, L_d = 0.6nH) for the forward-biased case, and as a series L_d-C_d (L_d = 0.6nH, C_d = 0.15 pF) network when reversed-biased. The fabricated prototype is driven by an Arduino microcontroller and it is illustrated in Fig. 10.

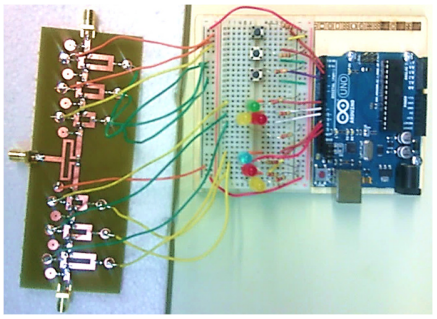

Fig. 10. Prototype of the feeding network that we have realized.

The comparison between the measured and simulated phase differences provided by the feeding line at Port#2 and Port#3 is presented in Fig. 11. The measured S_{ij} parameters are reported in Fig. 12 for the different values of Δθ. The agreement with the simulated values is quite good although the measured values are slightly lower than the simulations. This is probably due to a greater diode resistance (R_d) determined by the soldering process and by component tolerances.

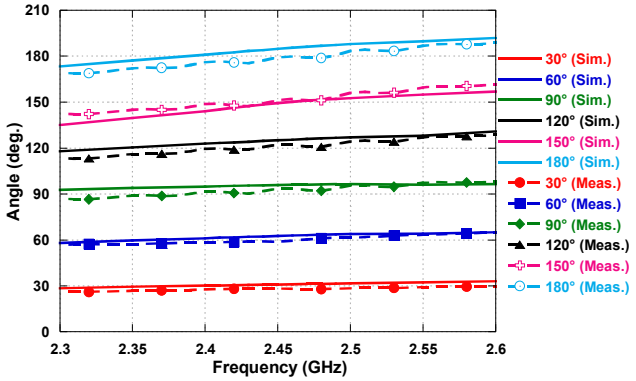

Fig. 11. Comparison between simulated and measured phase difference Δθ between Port#2 and Port#3.

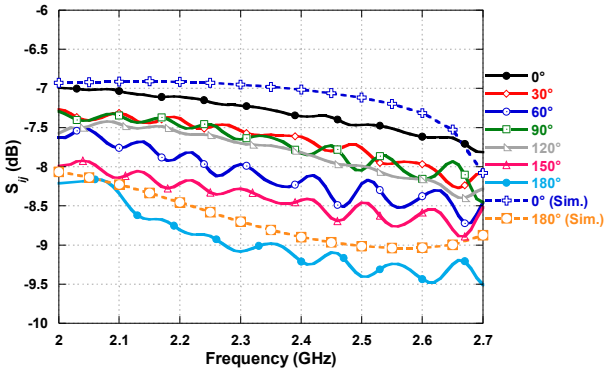

Fig. 12. Measured S_{ij} parameters as a function of the feeding network phase shift Δθ.

IV. Antenna Measurement

All the previous considerations provided the necessary building blocks to transform the antenna template into the final structure presented in Fig. 13. The realized feeding network is placed at the bottom of the FR4 substrate (1.2 mm thick)

whereas the upper part of the dielectric slab is the conducting plane. The CCEs are also printed on a FR4 single-sided copper substrate with the same thickness of 1.2 mm. The CCEs are connected to the feeding network through a via connection. The manufactured prototype is shown in Fig. 14. Nylon spacers and screws has been also used in order to keep the exciters at the exact distance of 4 mm from the ground plane.

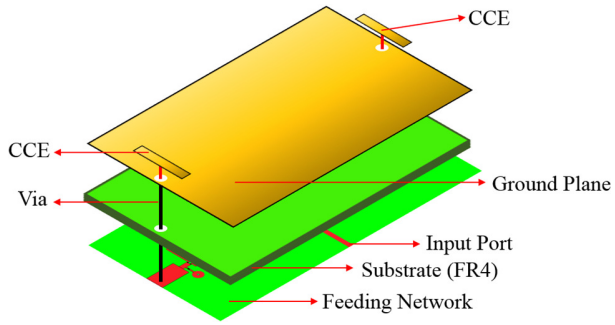

Fig. 13. Exploded 3D view of the antenna layout.

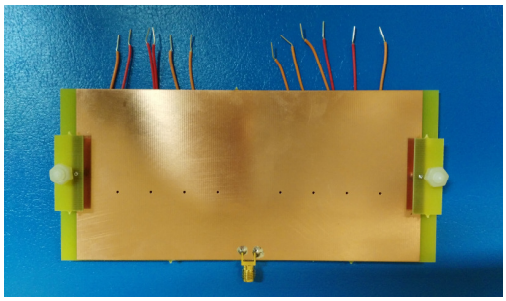

Fig. 14. Prototype of the manufactured antenna.

The comparisons between simulated and measured normalized radiation patterns on the *y-z* plane, are presented in Fig. 15 for different values of Δθ at 2.45 GHz. The measurements are in good agreement with the simulations and assess the reliability of the described design strategy. More in detail, it is apparent that by changing the phase difference between the two CCEs the pattern null points along the direction estimated in the simulations.

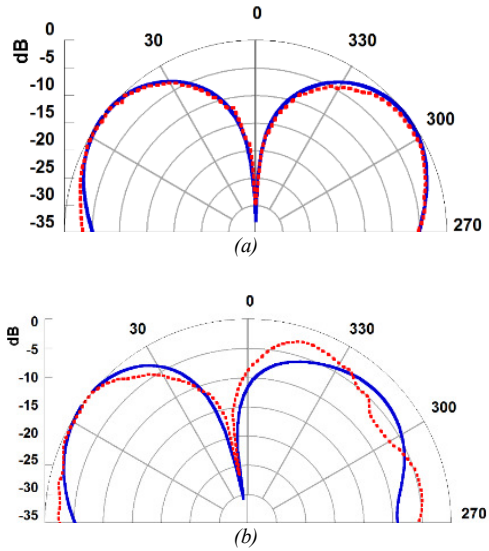

(a) *(b)*

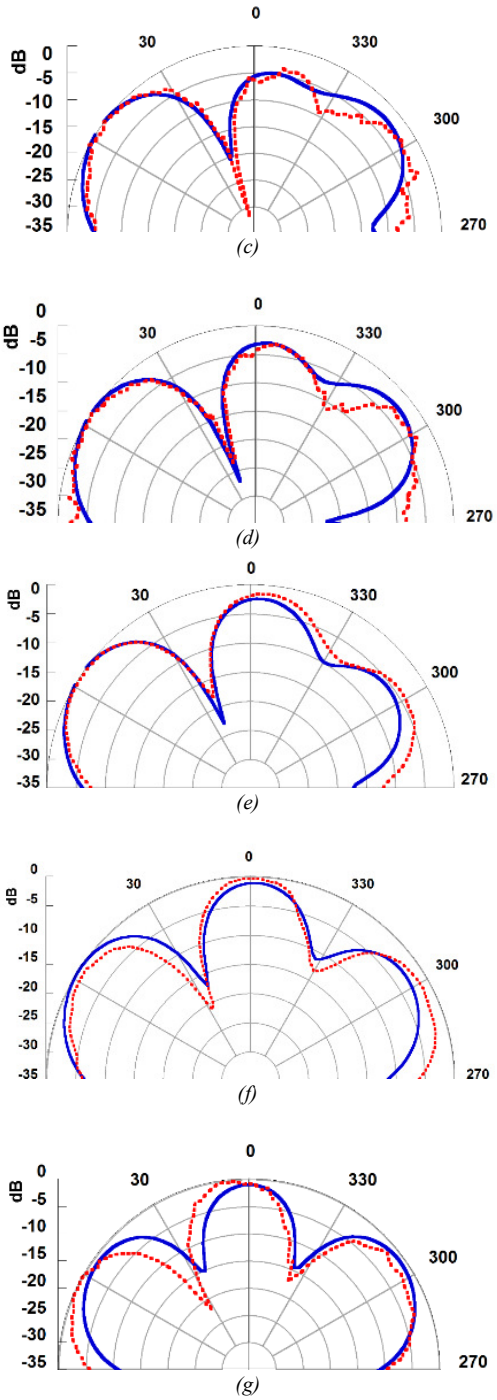

(c) *(d)* *(e)* *(f)* *(g)*

Fig. 15. Comparison between simulated (continuous line) and measured (dashed lines) normalized radiated pattern by changing the phase shift at 2.45 GHz, *(a)* Δθ =0°, *(b)* Δθ =30°, *(c)* Δθ =60°, *(d)* Δθ =90°, *(e)* Δθ =120°, *(f)* Δθ =150°, *(g)* Δθ =180°.

The agreement between simulations and measurements confirms that CCEs are able to excite only the two modes (*Mode#4* and *Mode#8*) found by resorting to the CMA. It is also apparent that it is possible to modify the level of excitation of these modes by using the asymmetric excitation.

Table I summarizes the measured scan angles and null depths as a function of phase difference Δθ. It can be observed that the null depth is always greater than 18 dB and that the null

can be placed within a beam of 64° centered at broadside direction (θ = 0°). The variation of the radiation pattern with respect to the frequency has been also investigated but the radiation pattern does not undergo significant changes in terms of the null- position within the considered range (2.4 – 2.5 GHz). A continuous null-scan can be achieved by using a different technological realization of the phase shifter [31].

TABLE I
MEASURED SCAN ANGLE AND NULL DEPTH AT 2.45 GHz

Delta Phase (deg.)	Scan Angle (deg.)	Null Depth (dB)
0	0	33.3
30	11	26.5
60	15	31
90	17	27
120	22	18
150	28	21
180	32	21

Finally, the measured and simulated reflection coefficients (S_{11}) are shown in Fig. 16 for all the investigated values of Δθ. The antenna is well matched within the frequency range of interest. The measured values are in good agreement with the simulations although some discrepancies are probably due to soldering effects and components tolerances that may cause a different biasing current (I_d) with respect the simulation, hence a different diode resistance (R_d).

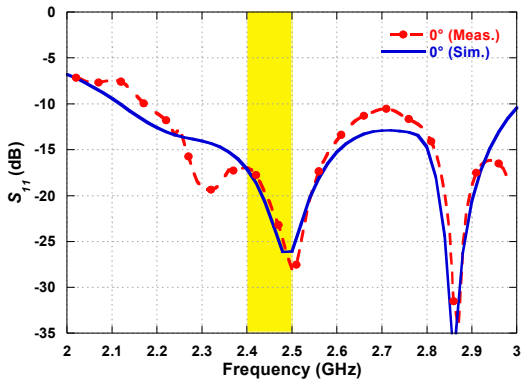

(a)

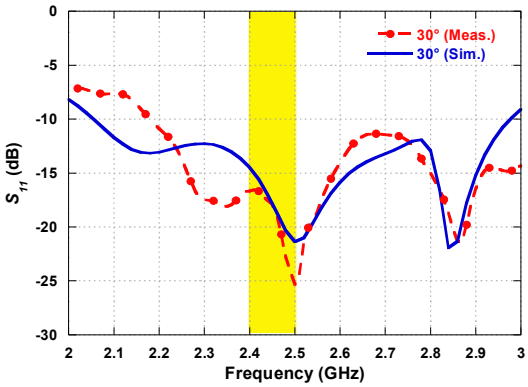

(b)

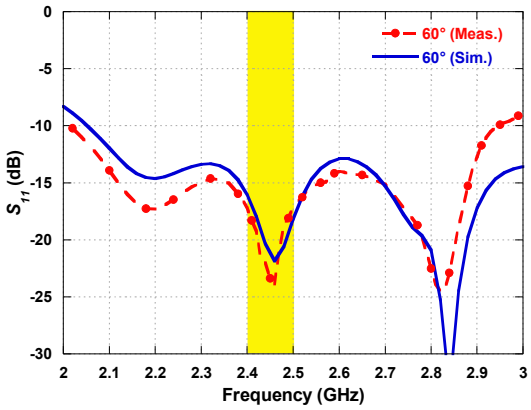

(c)

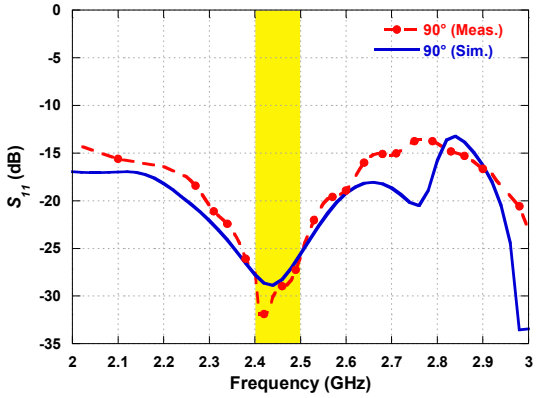

(d)

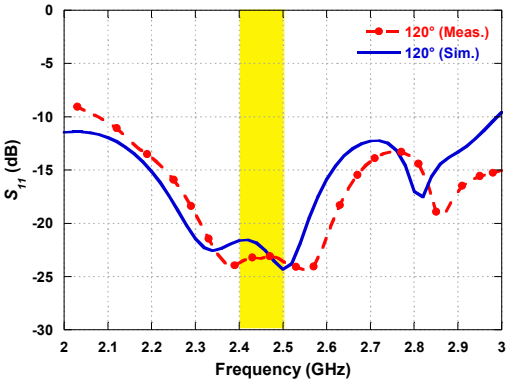

(e)

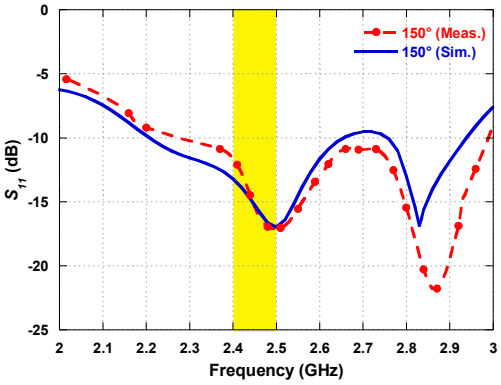

(f)

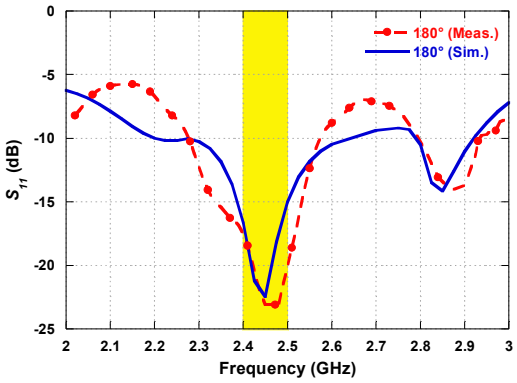

(g)

Fig. 16. Comparison between simulated and measured S_{11} parameter as a function of frequency by changing the phase shift; $\Delta\theta$ =0°, *(b)* $\Delta\theta$ =30°, *(c)* $\Delta\theta$ =60°, *(d)* $\Delta\theta$ =90°, *(e)* $\Delta\theta$ =120°, *(f)* $\Delta\theta$ =150°, *(g)* $\Delta\theta$ =180°.

V. Conclusion

A novel approach based on the CMA has been proposed for the design of null-scanning antennas. More in detail, the CMA allows to individuate the most promising current modes that can contribute to the desired pattern. The choice of the location and shape of the exciter has been addressed by evaluating the MWC and observing both amplitude and phase of the current modes. The phase relation between some of the modes has been exploited in order to achieve the null in the radiation pattern and it has been obtained with an asymmetric feeding of the employed exciters.

A novel low-cost null-steering antenna operating at 2.45 GHz has designed by using the aforementioned method. In particular, the proposed antenna allows a null shift of the radiation pattern by changing the relative phase between the two capacitive exciters (CCEs) located above the conductive plane. As a proof of concept, a prototype of the antenna has been realized by resorting to a discrete phase shifter employing pin diodes in order to scan the null. The measurements prove that by changing the phase difference $\Delta\theta$ between the two capacitive coupling CCEs the antenna scans up to 32° off broadside direction with a null depth greater than 18 dB is achieved. A continuous beam null-steering can be implemented as well by using a continuous phase shifter.

By following the same design flow, other structures can exploit their intrinsic Characteristic Modes to produce different shapes of the radiation pattern.

References

[1] S. Genovesi, A. D. Candia, and A. Monorchio, "Compact and Low Profile Frequency Agile Antenna for Multistandard Wireless Communication Systems," *IEEE Trans. Antennas Propag.*, vol. 62, no. 3, pp. 1019–1026, Mar. 2014.

[2] S. Genovesi, A. Monorchio, M. B. Borgese, S. Pisu, and F. M. Valeri, "Frequency-Reconfigurable Microstrip Antenna With Biasing Network Driven by a PIC Microcontroller," *IEEE Antennas Wirel. Propag. Lett.*, vol. 11, pp. 156–159, 2012.

[3] G. H. Huff and J. T. Bernhard, "Integration of Packaged RF MEMS Switches With Radiation Pattern Reconfigurable Square Spiral Microstrip Antennas," *IEEE Trans. Antennas Propag.*, vol. 54, no. 2, pp. 464–469, Feb. 2006.

[4] W. Lin and H. Wong, "Polarization Reconfigurable Wheel-Shaped Antenna With Conical-Beam Radiation Pattern," *IEEE Trans. Antennas Propag.*, vol. 63, no. 2, pp. 491–499, Feb. 2015.

[5] C. G. Christodoulou, Y. Tawk, S. A. Lane, and S. R. Erwin, "Reconfigurable Antennas for Wireless and Space Applications," *Proc. IEEE*, vol. 100, no. 7, pp. 2250–2261, Jul. 2012.

[6] B. A. Cetiner, H. Jafarkhani, J.-Y. Qian, H. J. Yoo, A. Grau, and F. De Flaviis, "Multifunctional reconfigurable MEMS integrated antennas for adaptive MIMO systems," *Commun. Mag. IEEE*, vol. 42, no. 12, pp. 62–70, 2004.

[7] S. Yong and J. T. Bernhard, "A Pattern Reconfigurable Null Scanning Antenna," *IEEE Trans. Antennas Propag.*, vol. 60, no. 10, pp. 4538–4544, Oct. 2012.

[8] S. Yong and J. T. Bernhard, "Reconfigurable Null Scanning Antenna With Three Dimensional Null Steer," *IEEE Trans. Antennas Propag.*, vol. 61, no. 3, pp. 1063–1070, Mar. 2013.

[9] M. S. Parihar, A. Basu, and S. K. Koul, "Efficient Spurious Rejection and Null Steering Using Slot Antennas," *IEEE Antennas Wirel. Propag. Lett.*, vol. 10, pp. 207–210, 2011.

[10] C. Deng, Y. Li, Z. Zhang, and Z. Feng, "A Hemispherical 3-D Null Steering Antenna for Circular Polarization," *IEEE Antennas Wirel. Propag. Lett.*, vol. 14, pp. 803–806, 2015.

[11] R. J. Garbacz and R. Turpin, "A generalized expansion for radiated and scattered fields," *IEEE Trans. Antennas Propag.*, vol. 19, no. 3, pp. 348–358, Maggio 1971.

[12] R. F. Harrington and J. R. Mautz, "Theory of characteristic modes for conducting bodies," *IEEE Trans. Antennas Propag.*, vol. 19, no. 5, pp. 622–628, Settembre 1971.

[13] E. Safin and D. Manteuffel, "Reconstruction of the Characteristic Modes on an Antenna Based on the Radiated Far Field," *IEEE Trans. Antennas Propag.*, vol. 61, no. 6, pp. 2964–2971, Jun. 2013.

[14] M. Cabedo-Fabres, E. Antonino-Daviu, A. Valero-Nogueira, and M. F. Bataller, "The theory of characteristic modes revisited: A contribution to the design of antennas for modern applications," *Antennas Propag. Mag. IEEE*, vol. 49, no. 5, pp. 52–68, 2007.

[15] K. A. Obeidat, B. D. Raines, R. G. Rojas, and B. T. Strojny, "Design of Frequency Reconfigurable Antennas Using the Theory of Network Characteristic Modes," *IEEE Trans. Antennas Propag.*, vol. 58, no. 10, pp. 3106–3113, Oct. 2010.

[16] A. Araghi and G. Dadashzadeh, "Oriented Design of an Antenna for MIMO Applications Using Theory of Characteristic Modes," *IEEE Antennas Wirel. Propag. Lett.*, vol. 11, pp. 1040–1043, 2012.

[17] Shen Wang and H. Arai, "Analysis of an Optimized Notch Array Antenna by Using the Theory of Characteristic Modes," *IEEE Antennas Wirel. Propag. Lett.*, vol. 13, pp. 253–256, 2014.

[18] R. Rezaiesarlak and M. Manteghi, "Design of Chipless RFID Tags Based on Characteristic Mode Theory (CMT)," *IEEE Trans. Antennas Propag.*, vol. 63, no. 2, pp. 711–718, Feb. 2015.

[19] R. Martens, E. Safin, and D. Manteuffel, "Inductive and capacitive excitation of the characteristic modes of small terminals," in *Antennas and Propagation Conference (LAPC), 2011 Loughborough*, 2011, pp. 1–4.

[20] D. Manteuffel and R. Martens, "Systematic design method of a mobile multiple antenna system using the theory of characteristic modes," *IET Microw. Antennas Propag.*, vol. 8, no. 12, pp. 887–893, Sep. 2014.

[21] R. Valkonen, A. Lehtovuori, and D. Manteuffel, "Capacitive coupling elements—Changing the way of designing antennas," in *Antennas and Propagation (EuCAP), 2014 8th European Conference on*, 2014, pp. 229–233.

[22] R. Martens, J. Holopainen, E. Safin, J. Ilvonen, and D. Manteuffel, "Optimal Dual-Antenna Design in a Small Terminal Multiantenna System," *IEEE Antennas Wirel. Propag. Lett.*, vol. 12, pp. 1700–1703, 2013.

[23] H. Li, Y. Tan, B. K. Lau, Z. Ying, and S. He, "Characteristic Mode Based Tradeoff Analysis of Antenna-Chassis Interactions for Multiple Antenna Terminals," *IEEE Trans. Antennas Propag.*, vol. 60, no. 2, pp. 490–502, Feb. 2012.

[24] H. Li, Z. T. Miers, and B. K. Lau, "Design of Orthogonal MIMO Handset Antennas Based on Characteristic Mode Manipulation at Frequency Bands Below 1 GHz," *IEEE Trans. Antennas Propag.*, vol. 62, no. 5, pp. 2756–2766, May 2014.

[25] Z. Miers, H. Li, and B. K. Lau, "Design of Bandwidth-Enhanced and Multiband MIMO Antennas Using Characteristic Modes," *IEEE Antennas Wirel. Propag. Lett.*, vol. 12, pp. 1696–1699, 2013.

[26] I. Szini, A. Tatomirescu, and G. F. Pedersen, "On Small Terminal MIMO Antennas, Harmonizing Characteristic Modes With Ground Plane Geometry," *IEEE Trans. Antennas Propag.*, vol. 63, no. 4, pp. 1487–1497, Apr. 2015.
[27] K. K. Kishor and S. V. Hum, "A two-port chassis-mode MIMO antenna," *Antennas Wirel. Propag. Lett. IEEE*, vol. 12, pp. 690–693, 2013.
[28] K. Kumar Kishor and S. V. Hum, "A Pattern Reconfigurable Chassis-Mode MIMO Antenna," *IEEE Trans. Antennas Propag.*, vol. 62, no. 6, pp. 3290–3298, Jun. 2014.
[29] J. Villanen, J. Ollikainen, O. Kivekas, and P. Vainikainen, "Coupling Element Based Mobile Terminal Antenna Structures," *IEEE Trans. Antennas Propag.*, vol. 54, no. 7, pp. 2142–2153, Jul. 2006.
[30] N. L. Bohannon and J. T. Bernhard, "Design Guidelines Using Characteristic Mode Theory for Improving the Bandwidth of PIFAs," *IEEE Trans. Antennas Propag.*, vol. 63, no. 2, pp. 459–465, Feb. 2015.
[31] S.-R. Ryu, H. Vardhan, B. Banerjee, and R. Prakash, "Continuous Active Phase Shifter Design and Analysis for Millimeter-Wave Circuits," *IEEE Trans. Circuits Syst. II Express Briefs*, vol. 60, no. 10, pp. 627–631, Oct. 2013.